

A model of photosynthetic CO₂ assimilation in C₃ leaves accounting for respiration and energy recycling by the plastidial oxidative pentose phosphate pathway

Thomas Wieloch¹ , Angela Augusti²  and Jürgen Schleucher³ 

¹Department of Forest Genetics and Plant Physiology, Swedish University of Agricultural Sciences, Umeå Plant Science Centre, 90183 Umeå, Sweden; ²Research Institute on Terrestrial Ecosystems, National Research Council, 05010 Porano, TR, Italy; ³Department of Medical Biochemistry and Biophysics, Umeå University, 90187 Umeå, Sweden

Summary

Author for correspondence:
Thomas Wieloch
Email: thomas.wieloch@slu.se

Received: 4 July 2022
Accepted: 13 April 2023

New Phytologist (2023) **239**: 518–532
doi: 10.1111/nph.18965

Key words: ATP : NADPH ratio, Calvin–Benson cycle, CO₂ mesophyll conductance, day respiration, Farquhar–von Caemmerer–Berry photosynthesis model, glucose–6-phosphate shunt, net CO₂ assimilation, oxidative pentose phosphate pathway.

- Recently, we reported estimates of anaplerotic carbon flux through the oxidative pentose phosphate pathway (OPPP) in chloroplasts into the Calvin–Benson cycle. These estimates were based on intramolecular hydrogen isotope analysis of sunflower leaf starch. However, the isotope method is believed to underestimate the actual flux at low atmospheric CO₂ concentration (C_a).
- Since the OPPP releases CO₂ and reduces NADP⁺, it can be expected to affect leaf gas exchange under both rubisco- and RuBP-regeneration-limited conditions. Therefore, we expanded Farquhar–von Caemmerer–Berry models to account for OPPP metabolism. Based on model parameterisation with values from the literature, we estimated OPPP-related effects on leaf carbon and energy metabolism in the sunflowers analysed previously.
- We found that flux through the plastidial OPPP increases both above and below $C_a \approx 450$ ppm (the condition the plants were acclimated to). This is qualitatively consistent with our previous isotope-based estimates, yet gas-exchange-based estimates are larger at low C_a .
- We discuss our results in relation to regulatory properties of the plastidial and cytosolic OPPP, the proposed variability of CO₂ mesophyll conductance, and the contribution of day respiration to the A/C_i curve drop at high C_a . Furthermore, we critically examine the models and parameterisation and derive recommendations for follow-up studies.

Introduction

Anaplerotic carbon flux into the Calvin–Benson cycle (CBC; for a list of abbreviations and symbols see Table 1) can occur by two metabolic pathways (Fig. 1). The first pathway (here denoted as cytosolic pathway) was proposed by Eicks *et al.* (2002) on discovering the xylulose-5-phosphate/phosphate translocator in *Arabidopsis thaliana*. This translocator enables the exchange of pentose phosphates and inorganic phosphate between chloroplasts and the cytosol. Screening *Arabidopsis* genome databases, Eicks *et al.* (2002) found genes encoding for the cytosolic oxidative branch of the pentose phosphate pathway (OPPP) as well as cytosolic ribulose-5-phosphate epimerase and ribose-5-phosphate isomerase. Genes encoding for cytosolic transketolase and transaldolase required to process pentose phosphates were missing. Because of the apparent lack of fate for pentose phosphates in the cytosol, Eicks *et al.* (2002) proposed their translocation into chloroplasts and injection into the CBC. Recently, studies on *Camelina sativa* leaf metabolism reported that this pathway carries high flux (*c.* 5% relative to net CO₂ assimilation, A) and supplies significant amounts of cytosolic NADPH (*c.* 10% relative to A) at an atmospheric CO₂ concentration (C_a) of *c.* 400 ppm (Wieloch & Sharkey, 2022; Xu *et al.*, 2022).

The second pathway (here denoted as plastidial pathway) was proposed by Sharkey & Weise (2016). It involves glucose 6-phosphate (G6P) to ribulose 5-phosphate (Ru5P) conversion by the plastidial OPPP and injection of the latter into the CBC. For *Pinus nigra*, we reported evidence consistent with flux through this pathway under drought (Wieloch *et al.*, 2018, 2022b). In sunflower, significant flux occurs when plants raised at $C_a \approx 450$ ppm are moved into low or high C_a (*c.* 180, 280, 700, 1500 ppm) whereas flux at $C_a \approx 450$ ppm was not significantly greater than zero (Wieloch, 2022; Wieloch *et al.*, 2022a). By contrast, Xu *et al.* (2021) reported, in *Camelina sativa*, significant flux occurs at $C_a \approx 400$ ppm corresponding to the conditions the plants were raised in. However, several assumptions of this study were criticised (Wieloch, 2021) and, after implementing amendments, the result was not confirmed (Xu *et al.*, 2022).

In sunflower, we estimated flux through the plastidial anaplerotic pathway based on a hydrogen isotope signal in leaf starch (the term isotope signal denotes systematic variability in relative isotope abundance; Wieloch, 2022; Wieloch *et al.*, 2022a). Assuming 50% of the net assimilated carbon becomes leaf starch (Sharkey *et al.*, 1985), anaplerotic flux proceeds at > 7%, > 5%, 0%, *c.* 2% and *c.* 5% relative to A at $C_a \approx 180, 280, 450, 700$ and 1500 ppm, respectively (Wieloch, 2022). However, this

Table 1 List of abbreviations and symbols.

Abbreviation	Definition
CBC	Calvin–Benson cycle
F6P	Fructose 6-phosphate
FvCB	Farquhar-von Caemmerer–Berry
G6P	Glucose 6-phosphate
G6PD	Glucose-6-phosphate dehydrogenase
OPPP	Oxidative branch of the pentose phosphate pathway
PGI	Phosphoglucose isomerase
Ru5P	Ribulose 5-phosphate
RuBP	Ribulose 1,5-bisphosphate
Symbol	Definition
A	Rate of net CO ₂ assimilation
A_c	Rate of rubisco-limited CO ₂ assimilation
A_j	Rate of RuBP-regeneration-limited CO ₂ assimilation
A_m	Measured net CO ₂ assimilation
abs	Absorptance of leaves
C_a	Atmospheric CO ₂ concentration
C_c	CO ₂ partial pressure or concentration at the active site of rubisco
C_i	CO ₂ partial pressure or concentration in intercellular air spaces
g_m	CO ₂ mesophyll conductance
I	Incident photon flux
I_2	Incident quanta utilised in electron transport through photosystem II
J	Rate of linear electron transport
$J_{a,p}$	Rate of electron recycling by the plastidial anaplerotic pathway
J_{max}	Light-saturated rate of linear electron transport
K_c	Michaelis–Menten constants of rubisco carboxylation
K_o	Michaelis–Menten constants of rubisco oxygenation
O_c	Oxygen partial pressure at the active site of rubisco
R_d	Rate of day respiration
$R_{a,p}$	Rate of respiration by and flux through the plastidial anaplerotic pathway
R_x	Rate of respiration by pathways other than the plastidial anaplerotic pathway
$S_{c/o}$	Relative CO ₂ /O ₂ specificity of rubisco
T	Temperature
V_c	Rubisco carboxylation rate
V_{cmax}	CO ₂ -saturated maximum rate of rubisco carboxylation
V_o	Rubisco oxygenation rate
Γ^*	CO ₂ -compensation point in the absence of day respiration
ΔA_j	Absolute effect of flux through the plastidial anaplerotic pathway on A/C_i curves
θ	Empirical curvature factor of the light response of electron transport
Φ	$V_o : V_c$ ratio

method is thought to strongly underestimate flux at 180 and 280 ppm because much of the hydrogen isotope signal can be expected to not arrive in starch under low- C_a conditions (Wieloch *et al.*, 2022a). Therefore, the present study aimed first and foremost at developing an alternative method for estimating flux through the plastidial anaplerotic pathway and second at exploring its capabilities.

For each molecule Ru5P synthesised anaplerotically, one molecule CO₂ is released from metabolism while two molecules NADP⁺ are reduced (Fig. 1). Thus, we hypothesise anaplerotic flux affects leaf gas exchange and can be traced by gas exchange modelling. To test this, we expand Farquhar-von Caemmerer–Berry (FvCB) photosynthesis models by terms accounting for anaplerotic respiration and energy recycling. Using gas exchange data of sunflower, we estimate anaplerotic flux rates and associated effects on leaf carbon and energy metabolism. These data are unique in that they were collected during the same experiment and from the same plants that previously provided isotope evidence for flux through the plastidial anaplerotic pathway (Wieloch, 2022; Wieloch *et al.*, 2022a). The results are discussed (*inter alia*) in relation to: previously reported flux estimates; regulatory properties of the plastidial and cytosolic anaplerotic pathway; the proposed variability of CO₂ mesophyll conductance (g_m) with C_a and during photosynthetic induction; and the contribution of day respiration to the often-seen A/C_i curve drop at high C_a (C_i , CO₂ concentration in intercellular air spaces). We close with a paragraph about weaknesses of the developed models and the chosen parameterisation and future research directions.

Description

Photosynthesis models accounting for anaplerotic flux into the Calvin–Benson cycle

In FvCB photosynthesis models (Farquhar *et al.*, 1980), net CO₂ assimilation is given as

$$A = V_c - 0.5V_o - R_d = V_c(1 - 0.5\Phi) - R_d \quad \text{Eqn 1}$$

where R_d denotes day respiration, V_o and V_c denote the oxygenation and carboxylation rates of ribulose 1,5-bisphosphate (RuBP), respectively, and Φ denotes the $V_o : V_c$ ratio. Making day respiration by the plastidial anaplerotic pathway ($R_{a,p}$) explicit yields

$$A = V_c(1 - 0.5\Phi) - R_{a,p} - R_x \quad \text{Eqn 2}$$

where R_x denotes day respiration by pathways other than the plastidial anaplerotic pathway. Please note that we also use $R_{a,p}$ to denote flux through the plastidial anaplerotic pathway.

Different biochemical processes may exert control over A . First, rubisco-limited CO₂ assimilation (A_c) denotes assimilation limited by CO₂ supply. Under these conditions, rubisco carboxylation rate is given as

$$V_c = \frac{V_{cmax}C_c}{C_c + K_c(1 + O_c/K_o)} \quad \text{Eqn 3}$$

where V_{cmax} denotes the CO₂-saturated maximum rate of rubisco carboxylation, C_c and O_c denote CO₂ and O₂ partial pressures at the active site of rubisco, respectively, and K_c and K_o denote the Michaelis–Menten constants of rubisco carboxylation and

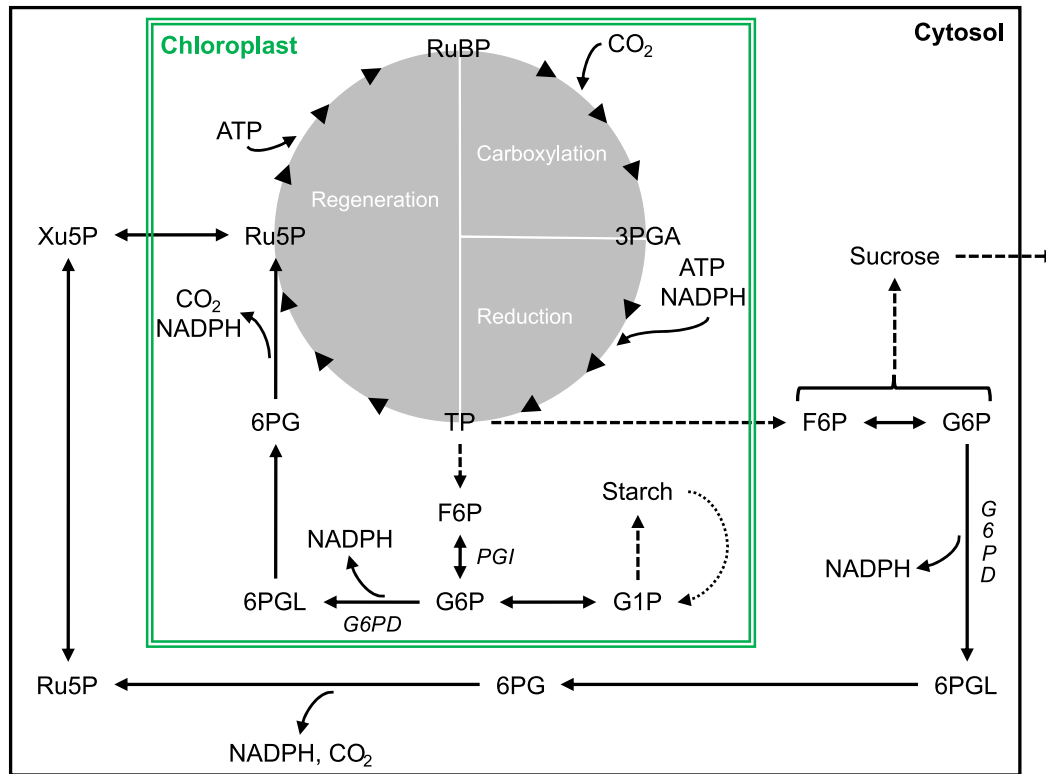


Fig. 1 Anaplerotic carbon flux into the Calvin–Benson cycle. Dotted arrow, phosphorolytic starch breakdown. 3PGA, 3-phosphoglycerate; 6PG, 6-phosphogluconate; 6PGL, 6-phosphogluconolactone; ATP, adenosine triphosphate; F6P, fructose 6-phosphate; FBP, fructose 1,6-bisphosphate; G1P, glucose 1-phosphate; G6P, glucose 6-phosphate; G6PD, glucose-6-phosphate dehydrogenase; NADPH, nicotinamide adenine dinucleotide phosphate; PGI, phosphoglucose isomerase; Ru5P, ribulose 5-phosphate; RuBP, ribulose 1,5-bisphosphate; TP, triose phosphate (glyceraldehyde 3-phosphate, dihydroxyacetone phosphate); Xu5P, xylulose 5-phosphate. Chloroplastic and cytosolic metabolism inside and outside the green box, respectively. Solid and dashed arrows represent transformations catalysed by a single enzyme or multiple enzymes, respectively.

oxygenation, respectively (Farquhar *et al.*, 1980). According to Farquhar & von Caemmerer (1982), Φ is related to the CO_2 -compensation point in the absence of day respiration (Γ_*) as

$$\Phi = \frac{2\Gamma_*}{C_c} \quad \text{Eqn 4}$$

Using Eqns 3, 4 to, respectively, remove V_c and Φ from Eqn 2 yields

$$A_c = \frac{V_{c\max}(C_c - \Gamma_*)}{C_c + K_c(1 + O_c/K_o)} - R_{a,p} - R_x \quad \text{Eqn 5}$$

Second, RuBP-regeneration-limited CO_2 assimilation (A_j) presumably results from a shortage of incoming electrons supplied to the CBC and photorespiration as NADPH and ATP (Farquhar *et al.*, 1980). Here, we assume NADPH rather than ATP supply is limiting. Electrons for NADP^+ reduction come from the linear electron transport pathway (1 mol NADPH requires 2 mol electrons). Additionally, per 1 mol CO_2 respired by anaplerotic pathways, 2 mol NADPH (4 mol electrons) are recycled (Fig. 1). However, only NADPH from the plastidial pathway can be recycled into the CBC and photorespiration. NADPH from the cytosolic pathway cannot enter chloroplasts

(Wieloch & Sharkey, 2022). Thus, overall electron supply is given as

$$e^- \text{ supply rate} = J + J_{a,p} = J + 4R_{a,p} \quad \text{Eqn 6}$$

where J denotes the rate of linear electron transport, and $J_{a,p}$ denotes the rate of electron recycling by the plastidial anaplerotic pathway. According to Farquhar *et al.* (1980), the rate of electron consumption by the CBC and photorespiration is given as

$$e^- \text{ consumption rate} = V_c(4 + 4\Phi) \quad \text{Eqn 7}$$

Balancing electron supply (Eqn 6) with electron consumption (Eqn 7) yields

$$J + 4R_{a,p} = V_c(4 + 4\Phi) \quad \text{Eqn 8}$$

Solving Eqn 8 for V_c yields

$$V_c = \frac{J + 4R_{a,p}}{4 + 4\Phi} \quad \text{Eqn 9}$$

Using Eqn 9 to remove V_c from Eqn 2 yields

$$A_j = \frac{J + 4R_{a,p}}{4 + 4\Phi} (1 - 0.5\Phi) - R_{a,p} - R_x \quad \text{Eqn 10}$$

CO₂ assimilation with electrons recovered by the plastidial anaplerotic pathway in the form of NADPH (Fig. 1) is given as

$$A_{a,p} = \frac{4R_{a,p}}{4 + 4\Phi} (1 - 0.5\Phi) = \frac{R_{a,p}}{1 + \Phi} (1 - 0.5\Phi) \quad \text{Eqn 11}$$

Using Eqn 4 to remove Φ from Eqn 10 yields

$$A_j = \frac{J + 4R_{a,p}}{4 + 8\Gamma_*/C_c} (1 - \Gamma_*/C_c) - R_{a,p} - R_x \quad \text{Eqn 12}$$

To quantify flux through the plastidial anaplerotic pathway and associated respiration, Eqn 12 is solved for $R_{a,p}$ as

$$R_{a,p} = - \frac{(A_j + R_x)(1 + 2\Gamma_*/C_c) - 0.25J(1 - \Gamma_*/C_c)}{3\Gamma_*/C_c} \quad \text{Eqn 13}$$

To calculate V_c , Φ is removed from Eqn 9 using Eqn 4 as

$$V_c = \frac{J + 4R_{a,p}}{4 + 8\Gamma_*/C_c} \quad \text{Eqn 14}$$

Using Φ (Eqn 4), V_o is calculated as

$$V_o = \Phi \times V_c = \frac{2\Gamma_* V_c}{C_c} \quad \text{Eqn 15}$$

Effects of respiration by the plastidial anaplerotic pathway on A/C_i curves

Respiration by the plastidial anaplerotic pathway can be expected to affect RuBP-regeneration-limited and rubisco-limited parts of A/C_i curves differently. In the following, effects associated with RuBP-regeneration-limited CO₂ assimilation are discussed first. Anaplerotic flux of 1 mol is associated with the release of 1 mol CO₂ and the supply of 2 mol NADPH (Fig. 1). In the complete absence of photorespiration, all this NADPH is used by the CBC (requires 2 NADPH per rubisco carboxylation) resulting in complete CO₂ reassimilation. Thus, in this theoretical scenario, A_j does not change in response to $R_{a,p}$, and gas exchange data do not convey any information on $R_{a,p}$ no matter how large $R_{a,p}$ is. By contrast, complete photorespiratory use of NADPH from the anaplerotic pathway (requires 2 NADPH per rubisco oxygenation) involves the release of 0.5 mol CO₂ by photorespiration per 1 mol CO₂ from the anaplerotic pathway (i.e. a total of 1.5 mol CO₂ is released). Thus, in the RuBP-regeneration-limited case, $R_{a,p}$ affects A/C_i curves because of photorespiration. The absolute effect of flux through the plastidial anaplerotic pathway on A/C_i curves (ΔA_j) is given as

$$\Delta A_j = 1.5R_{a,p} \frac{V_o}{V_c + V_o} = \frac{1.5\Phi R_{a,p}}{1 + \Phi} = \frac{3R_{a,p}}{2 + C_c/\Gamma_*} \quad \text{Eqn 16}$$

To calculate $R_{a,p}$ from observed A_j offsets, Eqn 16 is solved for $R_{a,p}$ as

$$R_{a,p} = \frac{\Delta A_j(1 + \Phi)}{1.5\Phi} = \frac{\Delta A_j(2 + C_c/\Gamma_*)}{3} \quad \text{Eqn 17}$$

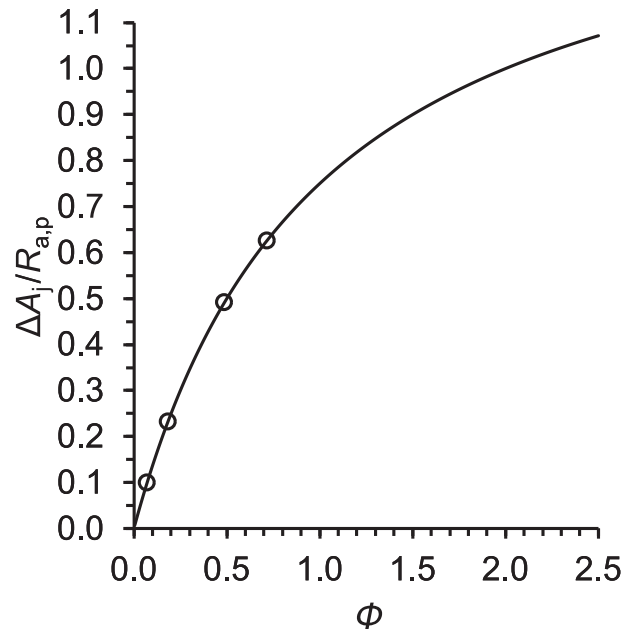


Fig. 2 Relative effect of respiration by the plastidial anaplerotic pathway on A/C_i curves under RuBP-regeneration-limited conditions ($\Delta A_j/R_{a,p}$) as function of the oxygenation-to-carboxylation ratio of rubisco (Φ). Black line: relationship based on theory (Eqn 18). Black circles: $\Delta A_j : R_{a,p}$ ratios pertaining to gas exchange data obtained from sunflower leaves at 300 $\mu\text{mol photons m}^{-2} \text{s}^{-1}$. ΔA_j denotes the observed difference between measured and modelled RuBP-regeneration-limited CO₂ assimilation where respiration by the plastidial anaplerotic pathway is not considered by the model (Fig. 4b, black dots vs red line). $R_{a,p}$ denotes respiration by the plastidial anaplerotic pathway estimated based on Eqn 13. RuBP, ribulose 1,5-bisphosphate.

The relative effect of respiration by the plastidial anaplerotic pathway on A/C_i curves is given as

$$\frac{\Delta A_j}{R_{a,p}} = \frac{1.5\Phi}{1 + \Phi} = \frac{3}{2 + C_c/\Gamma_*} \quad \text{Eqn 18}$$

Hence, the larger Φ , the larger the $\Delta A_j : R_{a,p}$ ratio (Fig. 2, black line). That is, the higher photorespiration, the larger the effect of respiration by the plastidial anaplerotic pathway on A/C_i curves. At $\Phi = 2$ (i.e. $C_c = \Gamma_*$, see Eqn 4), $\Delta A_j = R_{a,p}$ (i.e. $\Delta A_j/R_{a,p} = 1$). If $\Phi > 2$, then $\Delta A_j > R_{a,p}$. If $\Phi < 2$, then $\Delta A_j < R_{a,p}$.

Under rubisco-limited CO₂ assimilation, RuBP concentrations are above saturation level. Hence, NADPH from the anaplerotic pathway can be expected to exert no control on A_c . Shifts in $R_{a,p}$ will cause A_c shifts of the same size.

NADPH and ATP demand of plastidial carbon metabolism

NADPH demand by the CBC and photorespiration is given as (Farquhar *et al.*, 1980)

$$\text{NADPH demand} = 2V_c + 2V_o = V_c(2 + 2\Phi) \quad \text{Eqn 19}$$

This demand is met by NADPH supply from the light reactions. In the presence of flux through the plastidial anaplerotic pathway, NADPH demand from the light reactions is reduced as

$$NADPH\ demand = 2V_c + 2V_o - 2R_{a,p} = V_c(2 + 2\Phi) - 2R_{a,p} \quad \text{Eqn 20}$$

because anaplerotic flux of 1 mol is associated with the supply of 2 mol NADPH (Fig. 1).

Upon carboxylation of 1 mol RuBP, the CBC requires 3 mol ATP (Farquhar & von Caemmerer, 1982). Upon oxygenation of 1 mol RuBP, photorespiration requires 3 mol ATP in chloroplasts (1.5 mol by phosphoglycerate kinase, 1 mol by phosphoribulokinase and 0.5 mol by glycerate kinase). This accounting assumes that potentially harmful ammonium released by the mitochondrial glycine decarboxylase complex is immediately recaptured by mitochondrial (not plastidial) glutamine synthetase and then transported as glutamine to chloroplasts (Taira *et al.*, 2004; Buchanan *et al.*, 2015). ATP required by mitochondrial glutamine synthetase can be expected to come from mitochondrial oxidative phosphorylation. Hence, ATP demand by the CBC and photorespiration from the light reactions is given as

$$ATP\ demand = 3V_c + 3V_o = V_c(3 + 3\Phi) \quad \text{Eqn 21}$$

Combining Eqns 20 and 21, the ratio at which the CBC and photorespiration require ATP and NADPH is given as

$$\frac{ATP\ demand}{NADPH\ demand} = \frac{3V_c + 3V_o}{2V_c + 2V_o - 2R_{a,p}} = \frac{V_c(3 + 3\Phi)}{V_c(2 + 2\Phi) - 2R_{a,p}} \\ = \frac{1.5}{1 - R_{a,p}/(V_c + V_o)} \quad \text{Eqn 22}$$

Evidently, the CBC and photorespiration have the same plastidial cofactor demands with a plastidial ATP : NADPH demand ratio of 1.5. The ratio is independent of Φ . However, NADPH demands from the light reactions vary with $R_{a,p}$ resulting in varying relative demands of ATP and NADPH from the light reactions.

Materials and Methods

Samples and leaf gas exchange measurements

The sunflower (*Helianthus annuus* L.) samples were described previously (Ehlers *et al.*, 2015). In brief, the plants were raised in a glasshouse at $C_a \approx 450$ ppm and a light intensity of 300–400 $\mu\text{mol photons m}^{-2} \text{s}^{-1}$ (16 h photoperiod, 21% O_2). After 7–8 wk, they were transferred to a growth chamber ($T = 22^\circ\text{C}$: 18°C , $rH = 60\% : 70\%$, day : night), kept in darkness for 1 d to drain the starch reserves (see notes S3 in Wieloch *et al.*, 2022a) and subsequently grown for 2 d in groups of 8 at C_a of either *c.* 180, 280, 450, 700 or 1500 ppm (300–400 $\mu\text{mol photons m}^{-2} \text{s}^{-1}$, 16 h photoperiod).

Leaf gas exchange measurements were described previously (Ehlers *et al.*, 2015; see notes S1 in Wieloch *et al.*, 2022a). In brief, the measurements were performed with a previously described system (Laik & Edwards, 1997) under conditions similar to those in the growth chamber ($C_a = 173, 269, 433, 675, 1431$ ppm; $T = 22 \pm 0.5^\circ\text{C}$; 300 $\mu\text{mol photons m}^{-2} \text{s}^{-1}$,

21% O_2). C_i values obtained from gas exchange measurements (136, 202, 304, 516 and 1282 ppm) are similar to C_i values estimated for the 2-d growth chamber experiments (140, 206, 328, 531 and 1365 ppm; see notes S2 in Wieloch *et al.*, 2022a). To constrain V_{cmax} , we additionally measured gas exchange at 900 $\mu\text{mol photons m}^{-2} \text{s}^{-1}$, $C_a = 173, 269, 432, 674$ and 1430 ppm corresponding to $C_i = 126, 188, 264, 450$ and 1204 ppm.

Parameterisation of photosynthesis models

C_c was calculated according to Fick's first law as

$$C_c = C_i - \frac{A}{g_m} \quad \text{Eqn 23}$$

using $g_m = 0.45 \text{ mol CO}_2 \text{ m}^{-2} \text{ s}^{-1}$ reported for sunflower at 20°C , 600 $\mu\text{mol photons m}^{-2} \text{ s}^{-1}$ (Schäufele *et al.*, 2011). For rubisco extracted from sunflower, Genkov *et al.* (2010) reported $K_c = 19 \mu\text{M CO}_2$, $K_o = 640 \mu\text{M O}_2$, and a relative CO_2/O_2 specificity ($S_{c/o}$) of 77 (M/M) at 25°C . Γ_* at 25°C was calculated based on published procedures (von Caemmerer, 2000) as

$$\Gamma_* = \frac{0.5 O_c}{S_{c/o}} \quad \text{Eqn 24}$$

with $O_c = 256 \mu\text{M}$. To convert from concentration to partial pressure, solubilities for CO_2 of $0.0334 \text{ mol l}^{-1} \text{ bar}^{-1}$ and O_2 of $0.00126 \text{ mol l}^{-1} \text{ bar}^{-1}$ were used. Since correction factors for sunflower are unavailable, we used Q_{10} values reported in table 2.3 of von Caemmerer (2000) and eqn 2.32 in von Caemmerer (2000) to correct for leaf temperature (22°C). This gave $K_c = 447 \mu\text{bar CO}_2$, $K_o = 439 \text{ mbar O}_2$ and $\Gamma_* = 45.3 \mu\text{bar CO}_2$. To estimate V_{cmax} , Eqn 5 was fitted to gas exchange data obtained at 900 $\mu\text{mol photons m}^{-2} \text{ s}^{-1}$, $C_a = 173, 269, 432$ ppm (Fig. 3). Under standard conditions (400 ppm CO_2 , 21% O_2 , 20– 25°C), R_d usually proceeds at *c.* 5% relative to the rate of A (Tcherkez *et al.*, 2017; Xu *et al.*, 2022). Fixing $R_{a,p} + R_x$ at this rate ($= 0.83 \mu\text{mol CO}_2 \text{ m}^{-2} \text{ s}^{-1}$), we found $V_{cmax} = 83.2 \mu\text{mol m}^{-2} \text{ s}^{-1}$. This is similar to a previously reported estimate for sunflower of 80 $\mu\text{mol m}^{-2} \text{ s}^{-1}$ at 20°C (Jacob & Lawlor, 1991; Wullschlegel, 1993).

Based on Farquhar & Wong (1984), J is given as

$$J = \frac{I_2 + J_{max} - \sqrt{(I_2 + J_{max})^2 - 4\theta I_2 J_{max}}}{2\theta} \quad \text{Eqn 25}$$

where θ denotes the empirical curvature factor of the light response of electron transport commonly set to 0.7 (Evans, 1989), J_{max} denotes the light-saturated rate of linear electron transport, and I_2 denotes incident quanta utilised in electron transport through photosystem II given as

$$I_2 = I \times \text{abs}(1-f)/2 \quad \text{Eqn 26}$$

where I denotes incident photon flux, abs denotes absorptance of leaves commonly set to 0.85, and f denotes a correction factor for the spectral quality of light commonly set to 0.15 (Evans, 1987).

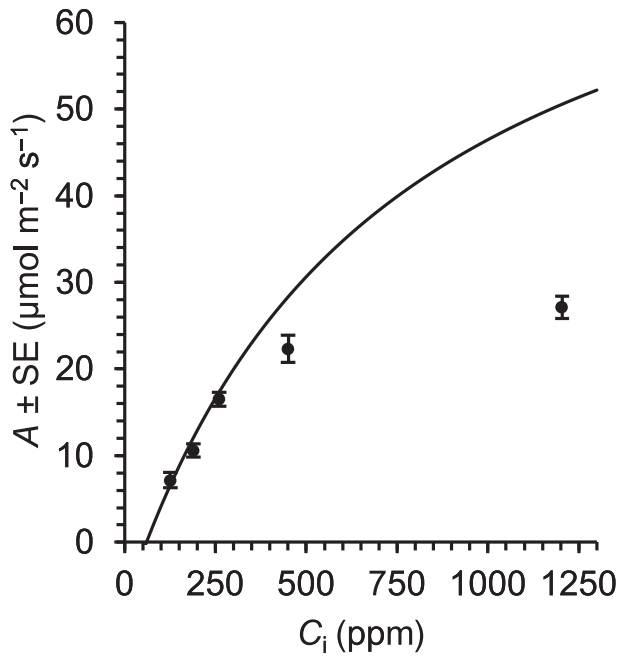


Fig. 3 Net CO₂ assimilation (A) of sunflower leaves as function of intercellular CO₂ concentration (C_i). Black dots: measured values (A_m , $n = 8$). Solid line: best fit between the data at $C_a = 173, 269, 432$ ppm and a model of rubisco-limited A (Eqn 5). Plants were raised in a glasshouse at an atmospheric CO₂ concentration (C_a) of c. 450 ppm and a light intensity of 300–400 $\mu\text{mol photons m}^{-2} \text{s}^{-1}$. Gas exchange measurements were performed at 22°C, 900 $\mu\text{mol photons m}^{-2} \text{s}^{-1}$, and atmospheric CO₂ concentrations of $C_a = 173, 269, 432, 674$ and 1430 ppm corresponding to intercellular CO₂ concentrations of $C_i = 126, 188, 264, 450$ and 1204 ppm. Model inputs: $C_c = 111, 168, 226$ μbar , $K_c = 447$ $\mu\text{bar CO}_2$, $K_o = 439$ mbar O₂, and $\Gamma^* = 45.3$ $\mu\text{bar CO}_2$, $O_c = 206$ 373 μbar , $R_{a,p} + R_x = 0.83$ $\mu\text{mol CO}_2 \text{m}^{-2} \text{s}^{-1}$. Model output: $V_{cmax} = 83.2$ $\mu\text{mol m}^{-2} \text{s}^{-1}$.

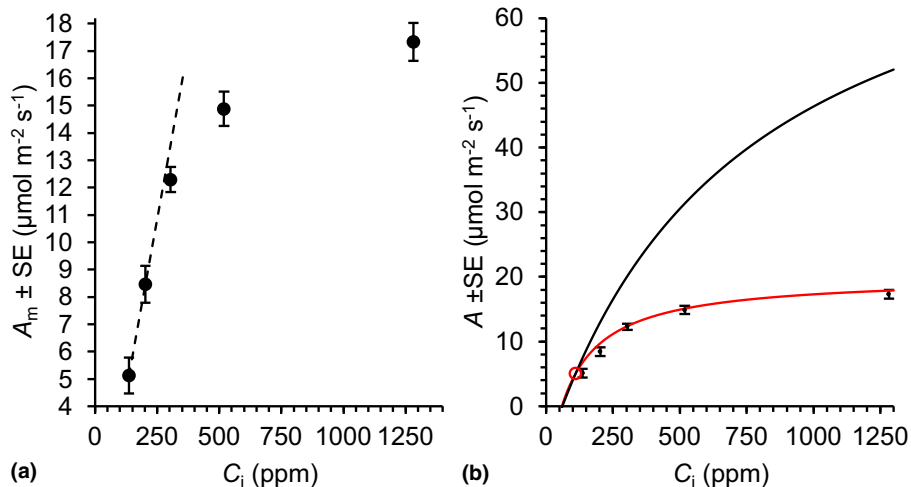


Fig. 4 Measured (a) and modelled (b) net CO₂ assimilation (A) of sunflower leaves as function of intercellular CO₂ concentration (C_i). Black dots: measured values (A_m , $n = 8$). Dashed black line: trendline passing through the two lowest A_m values. Solid black and red lines: modelled rubisco-limited assimilation (A_c) and RuBP-regeneration-limited assimilation (A_j), respectively (respiration by the plastidial anaplerotic pathway not considered). Red circle: intersection between A_c and A_j . Plants were grown in a glasshouse at an atmospheric CO₂ concentration (C_a) of c. 450 ppm and then moved to growth chambers. After a day in darkness to drain the starch reserves, plants were grown at different levels of C_a (180, 280, 450, 700 and 1500 ppm) corresponding to different levels of C_i (140, 206, 328, 531 and 1365 ppm) for 2 d. During gas exchange measurements, slightly lower C_i levels prevailed (136, 202, 304, 516 and 1282 ppm). A_j -model inputs: $\Gamma^* = 45.3$ $\mu\text{bar CO}_2$, $J_{max} = 168.3$ $\mu\text{mol m}^{-2} \text{s}^{-1}$, $\theta = 0.7$, $I = 300$ $\mu\text{mol photons m}^{-2} \text{s}^{-1}$, $abs = 0.85$ and $f = 0.15$. A_j -model output: $R_{a,p} + R_x = 0.96$ $\mu\text{mol CO}_2 \text{m}^{-2} \text{s}^{-1}$. A_c -model inputs: $K_c = 447$ $\mu\text{bar CO}_2$, $K_o = 439$ mbar O₂, and $\Gamma^* = 45.3$ $\mu\text{bar CO}_2$, $O_c = 207$ 548 μbar , $V_{cmax} = 83.2$ $\mu\text{mol m}^{-2} \text{s}^{-1}$, $R_{a,p} + R_x = 0.96$ $\mu\text{mol CO}_2 \text{m}^{-2} \text{s}^{-1}$. RuBP, ribulose 1,5-bisphosphate.

Since gas exchange data collected at very high irradiance are unavailable, J_{max} was estimated based on its close relationship with V_{cmax} according to published procedures (Walker *et al.*, 2014) as

$$\log_e(J_{max}) = \beta_1 + \beta_2 \log_e(V_{cmax}) \quad \text{Eqn 27}$$

Using parameter estimates pertaining to data reported by Wullschlegel (1993; $\beta_1 = 1.425$, $\beta_2 = 0.837$, $R^2 = 87.2$, $P < 0.001$, $n = 110$), we estimate $J_{max} = 168.3$ $\mu\text{mol m}^{-2} \text{s}^{-1}$.

Results

Metabolic phases of the A/C_i curve

A/C_i curves enable the identification of metabolic processes limiting net CO₂ assimilation (Farquhar *et al.*, 1980). Initial linear increases at low C_i are commonly attributed to rubisco-limited assimilation. A change point in the response of A to C_i marks the onset of RuBP-regeneration-limited assimilation. Furthermore, under high light, A/C_i curves may level out at high C_i which is commonly attributed to limited triose phosphate utilisation (Sharkey, 1985).

Despite the relatively low resolution of our A/C_i curve, two phases are evident (Fig. 4a). An initial linear increase (dashed line) is followed by RuBP-regeneration-limited assimilation whereas levelling out at high C_i is not evident. Hence, triose phosphate utilisation did not affect A_m (denoting measured net CO₂ assimilation). This is as expected considering the low irradiance applied during data collection (300 $\mu\text{mol photons m}^{-2} \text{s}^{-1}$).

Table 2 Rates of day respiration in sunflower leaves.

C_a (ppm)	A_m ($\mu\text{mol m}^{-2} \text{s}^{-1}$)	$A_j - A_m^a$ ($\mu\text{mol m}^{-2} \text{s}^{-1}$)	$R_{a,p}^b$ ($\mu\text{mol m}^{-2} \text{s}^{-1}$)	$R_{a,p}/A_m$ (%)	$R_{a,p}/A_m^d$ (%)	R_x^e ($\mu\text{mol m}^{-2} \text{s}^{-1}$)	R_x/A_m (%)
c. 180	5.13	1.73	2.75	53.7	> 7	0.96	18.8
c. 280	8.46	1.20	2.44	28.9	> 5	0.96	11.4
c. 450	12.29	0	0	0	0	0.96	7.8
c. 700	14.88	0.19	0.80 ^c	5.3 ^c	c. 2	1.08	7.2
c. 1500	17.33	0.51	5.03 ^c	29.0 ^c	c. 5	1.38	8.0

Plants were grown in a glasshouse at an atmospheric CO_2 concentration (C_a) of c. 450 ppm and then moved to growth chambers. After a day in darkness to drain the starch reserves, the plants were grown at different levels of C_a (180, 280, 450, 700 and 1500 ppm) corresponding to different levels of intercellular CO_2 concentration ($C_i = 140, 206, 328, 531$ and 1365 ppm) for 2 d. During gas exchange measurements, slightly lower C_i levels prevailed (136, 202, 304, 516 and 1282 ppm). Symbols: A_j , modelled ribulose 1,5-bisphosphate (RuBP)-regeneration-limited CO_2 assimilation; A_m , measured CO_2 assimilation; $R_{a,p}$, respiration by the plastidial anaplerotic pathway; R_x , day respiration by processes other than the plastidial anaplerotic pathway.

^a A_j estimates based on Eqn 28 with $R_x = 0.96 \mu\text{mol CO}_2 \text{ m}^{-2} \text{ s}^{-1}$.

^bEstimates based on gas exchange data (Eqn 13).

^cProbably overestimated (see text).

^dEstimates based on previously published isotope data (Wieloch, 2022).

^eEstimates based on Eqn 28 for $C_a \approx 180, 280$ and 450 ppm, and Eqn 29 for $C_a \approx 700$ and 1500 ppm.

Previously, we have shown that flux through the plastidial anaplerotic pathway is not significantly different from zero at $C_a \approx 450$ ppm (Wieloch, 2022; Wieloch *et al.*, 2022a). Hence, RuBP-regeneration-limited assimilation for this data point as derived from Eqn 12 is given as

$$A_j = \frac{J}{4 + 8\Gamma_*/C_c} (1 - \Gamma_*/C_c) - R_x \quad \text{Eqn 28}$$

which is equivalent to the original FvCB model. Eqn 28 was fitted to A_m by varying R_x until the offset between modelled and measured c. 450 ppm values was zero (Fig. 4b, red line). The condition was met at $R_x = 0.96 \mu\text{mol CO}_2 \text{ m}^{-2} \text{ s}^{-1}$. Hence, at c. 450 ppm, R_d proceeds at 7.8% relative to A_m , which agrees well with previous reports. Under standard conditions (400 ppm CO_2 , 21% O_2 , 20–25°C), leaf R_d commonly proceeds at $\geq 5\%$ relative to A_m (Tcherkez *et al.*, 2017). This agreement lends some credibility to the validity of our chosen model parameterisation.

Using $R_x = 0.96 \mu\text{mol CO}_2 \text{ m}^{-2} \text{ s}^{-1}$ and assuming $R_{a,p} = 0$, we next modelled rubisco-limited assimilation based on Eqn 5 (Fig. 4b, black line). Above $C_a \approx 133$ ppm ($C_i \approx 110$ ppm), we found that $A_c > A_j \geq A_m$ (Fig. 4b, black line vs red line vs black dots). This indicates that A_m at $C_a > 133$ ppm does not result from rubisco-limited but RuBP-regeneration-limited assimilation.

Effects of varying rates of day respiration on the A/C_i curve

Based on changes in hydrogen isotope fractionation in starch extracted from the leaves studied here, we previously estimated $R_{a,p}$ proceeds at > 7%, > 5%, 0%, c. 2% and c. 5% relative to A_m at $C_a \approx 180, 280, 450, 700$ and 1500 ppm, respectively (Table 2; Wieloch, 2022). That is, $R_{a,p}$ exhibits a change point in response to C_a at $C_a \approx 450$ ppm. Seeing that there are positive offsets between A_m and A_j both above and below $C_a \approx 450$ ppm (Table 2; Fig. 4b, red line vs black dots), this same change point appears to be present in A_m , and $R_{a,p}$ can be expected to contribute to the offsets.

Using Eqn 13, we estimate $R_{a,p}$ proceeds at 54%, 29%, 0%, 5% and 29% relative to A_m at $C_a \approx 180, 280, 450, 700$ and 1500 ppm, respectively (Table 2). Estimates at low C_a (c. 180, and 280 ppm) are consistent with isotope-derived estimates because, based on the properties of the biochemical system, the isotope approach can be expected to underestimate $R_{a,p}$ at low C_a (see Wieloch *et al.*, 2022a). By contrast, the isotope approach is believed to not strongly underestimate $R_{a,p}$ at high C_a (Wieloch, 2022). However, gas exchange estimates of $R_{a,p}$ at high C_a (c. 700, and 1500 ppm) are considerably larger than isotope-derived estimates. This may suggest that gas exchange modelling overestimates $R_{a,p}$ at high C_a .

Overestimation of $R_{a,p}$ at high C_a may derive from variability of R_x . To follow up on this, we solve the A_j model (Eqn 12) for R_x and substitute A_j by A_m as

$$R_x = \frac{J + 4R_{a,p}}{4 + 8\Gamma_*/C_c} (1 - \Gamma_*/C_c) - R_{a,p} - A_m \quad \text{Eqn 29}$$

Using isotope-derived $R_{a,p}$ values as inputs, we estimate that absolute rates of R_x increase from 450 to 1500 ppm while relative rates remain approximately constant (Table 2). Based on regulatory properties of leaf respiratory processes, this finding seems reasonable (see ‘Metabolic origin of day respiration at high C_a ’ in the Discussion section). Taken together, our results suggest A_m is a function of RuBP-regeneration-limited assimilation and variability of $R_{a,p}$ and R_x (Eqn 12). Fig. 5 summarises estimated carbon and associated NADPH fluxes. Uncertainties associated with these estimates are discussed below (see ‘Model criticism and future research directions’ in the Discussion section).

Integration of day respiration in carbon metabolism

Based on estimations and assumptions given above, $R_{a,p}$ proceeds at c. 54%, 29%, 0%, 2%, and 5% relative to A_m at $C_a \approx 180, 280, 450, 700$ and 1500 ppm, respectively (Fig. 6a). Thus, it governs R_d at low C_a (c. 73% contribution at c. 180, and 280

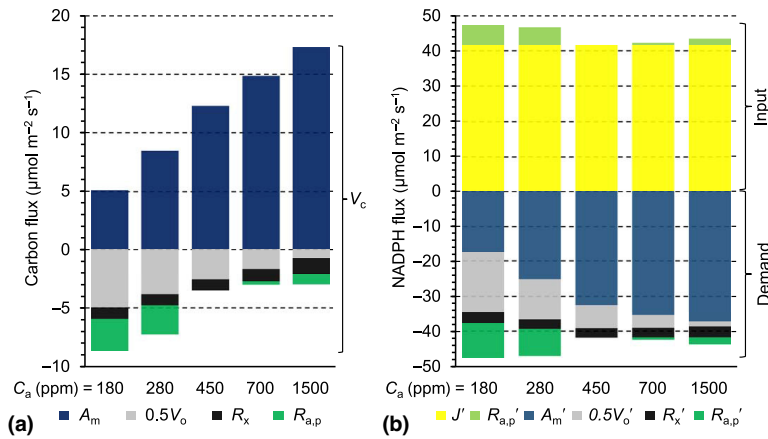


Fig. 5 Carbon (a) and NADPH fluxes (b) at varying atmospheric CO₂ concentration (C_a) in sunflower leaves. Estimates derived from modelling RuBP-regeneration-limited CO₂ assimilation. The model considers the Calvin–Benson cycle, the photorespiration cycle, the plastidial anaplerotic pathway and respiration by processes other than the plastidial anaplerotic pathway. Plants were grown in a glasshouse at C_a ≈ 450 ppm and then moved to growth chambers. After a day in darkness to drain the starch reserves, plants were grown at different levels of C_a (180, 280, 450, 700 and 1500 ppm) corresponding to different levels of C_i (140, 206, 328, 531 and 1365 ppm) for 2 d. During gas exchange measurements, slightly lower C_i levels prevailed (136, 202, 304, 516 and 1282 ppm). NADPH demands of individual carbon fluxes (see Fig. 5a) were calculated as (2 + 2Φ) × flux with flux = {−A_m; 0.5V_o; R_x; R_{a,p}}. Symbols: A_m, measured net CO₂ assimilation; A_m', NADPH demand of net CO₂ assimilation; J', NADPH supply by whole chain electron transport (0.5 J); R_{a,p}, respiration by the plastidial anaplerotic pathway; R_{a,p}', NADPH supply (light green) and demand (dark green) by the plastidial anaplerotic pathway; R_x', day respiration by processes other than the plastidial anaplerotic pathway; R_x', NADPH demand for assimilation of CO₂ respired by processes other than the plastidial anaplerotic pathway; V_c, rubisco carboxylation; 0.5V_o, photorespiratory CO₂ release; 0.5V_o', NADPH demand for assimilation of CO₂ respired by photorespiration; Φ, oxygenation-to-carboxylation ratio of rubisco; NADPH, nicotinamide adenine dinucleotide phosphate; RuBP, ribulose 1,5-bisphosphate.

ppm) and contributes substantially to R_d at high C_a (c. 22% at c. 700 ppm, and c. 39% at c. 1500 ppm; Fig. 6b). Taken together, R_d proceeds at c. 72%, 40%, 8%, 9%, and 13% relative to A_m at C_a ≈ 180, 280, 450, 700, and 1500 ppm, respectively (Table 2). While R_{a,p} exceeds photorespiratory CO₂ release at high C_a (c. 1500 ppm), it proceeds at > 55% relative to the rate of photorespiratory CO₂ release at low C_a (c. 180, and 280 ppm; Fig. 6c). Furthermore, R_{a,p} accounts for > 40% of the total CO₂ release at both low and high C_a (c. 180, 280, and 1500 ppm; Fig. 6d). At low C_a (c. 180, and 280 ppm), R_{a,p} accounts for > 15% of V_c (Fig. 6e) and thus causes significant futile carbon cycling involving CO₂ uptake by the CBC and release by the plastidial anaplerotic pathway. At the same C_a, > 10% of all RuBP is provided by the plastidial anaplerotic pathway (Fig. 6f). When plotted against A_m, R_{a,p} increases nonlinearly both below and above C_a ≈ 450 ppm (Fig. 6g). Towards very low A_m (< 5 µmol m⁻² s⁻¹, C_a < 180 ppm), R_{a,p} may approach a maximum. Above A_m = 12.3 µmol m⁻² s⁻¹ (C_a ≈ 450 ppm), R_{a,p} increases exceed R_x increases by approximately a factor of two (Fig. 6g,h).

Energy recovery by the plastidial anaplerotic pathway and associated CO₂ assimilation

NADPH inputs required to assimilate CO₂ respired by the plastidial anaplerotic pathway exceed NADPH outputs of this pathway (Table 3, Fig. 5). However, relative NADPH loss decreases as Φ decreases with relative NADPH recovery converging to one. Accordingly, CO₂ release by the anaplerotic pathway (R_{a,p}) exceeds CO₂ recovery with NADPH from the anaplerotic pathway (A_{a,p}, Table 3). Relative CO₂ recovery increases with decreasing Φ converging to one (A_{a,p}/R_{a,p}). Hence, R_{a,p} is larger than the effect that flux through the plastidial anaplerotic pathway has on

A/C_i curves (ΔA_j, Table 3). With decreasing Φ, the relative effect of flux through the plastidial anaplerotic pathway on the A/C_i curve decreases converging to zero (ΔA_j/R_{a,p}, Table 3, black circles in Fig. 2). Taken together, anaplerotic flux is energetically wasteful and thus decreases net CO₂ assimilation but this is partly offset by NADPH recovery. Recovered NADPH is most efficiently used for CO₂ recovery when photorespiration is low since photorespiration is energetically wasteful and releases additional CO₂ (see ‘Effects of respiration by the plastidial anaplerotic pathway on A/C_i curves’ in the Description section).

Effects of the plastidial anaplerotic pathway on the light reactions of photosynthesis

In the present study, light was maintained at 300 µmol photons m⁻² s⁻¹ across all C_a treatments. Accordingly, linear electron transport supplied a steady amount of NADPH (Fig. 5b, yellow bars). Above and below C_a ≈ 450 ppm, the plastidial anaplerotic pathway supplied additional NADPH yet no ATP (Fig. 5b, light green bars). Balancing the ensuing NADPH surplus with the demands of the CBC and photorespiration requires additional inputs of ATP from photophosphorylation (Fig. 7, black triangles). Hence, the ratio of ATP : NADPH demand from the light reactions increases both above and below C_a ≈ 450 ppm with increasing flux through the plastidial anaplerotic pathway (Fig. 7, red circles).

Assuming the synthesis of 3 mol ATP requires 12 mol H⁺ as derived from the thermodynamics of the ATPase reaction (Steigmiller *et al.*, 2008), we find that ATP : NADPH supply by linear electron transport including Q cycling is perfectly aligned with the demands of the CBC and photorespiration at C_a ≈ 450 ppm (Table 4, cf. Eqn 22). By contrast, assuming the synthesis of 3

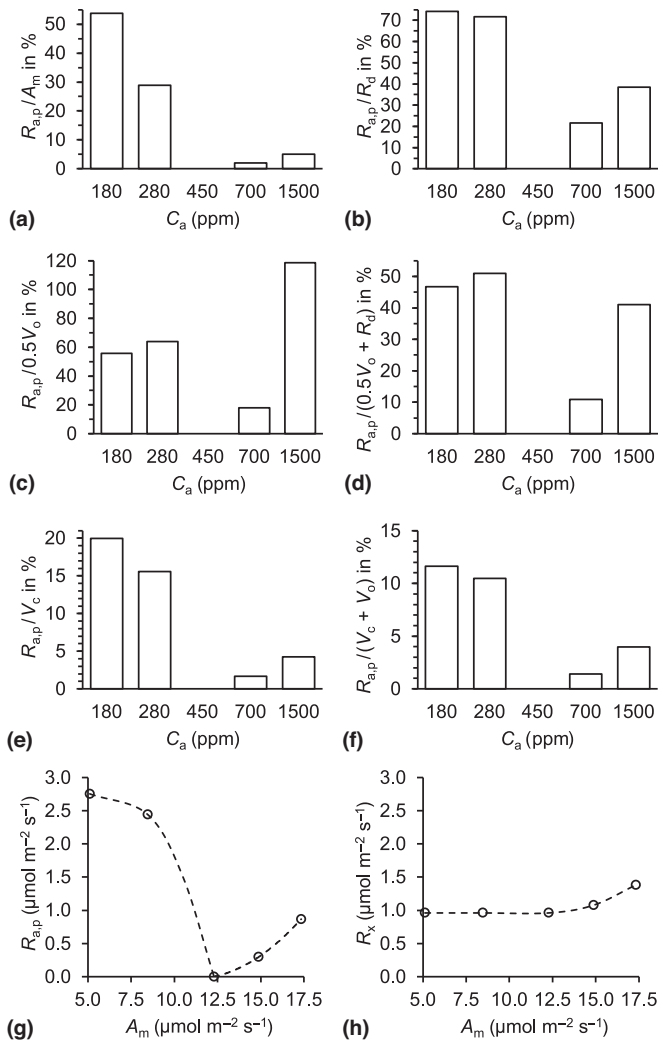


Fig. 6 Integration of day respiration in carbon metabolism of sunflower leaves. The rate of respiration by the plastidial anaplerotic pathway is shown relative to the rate of net CO₂ assimilation (a), the rate of day respiration (b), the rate of photorespiratory CO₂ release (c), the rate of total CO₂ release (d), the rate of rubisco carboxylation (e) and the combined rate of rubisco carboxylation and oxygenation (f). Furthermore, the rate of respiration by the plastidial anaplerotic pathway and the rate of respiration by processes other than the plastidial anaplerotic pathway are shown as function of the rate of net CO₂ assimilation (g and h). Plants were grown in a glasshouse at $C_a \approx 450$ ppm and then moved to growth chambers. After a day in darkness to drain the starch reserves, plants were grown at different levels of C_a (180, 280, 450, 700 and 1500 ppm) corresponding to different levels of C_i (140, 206, 328, 531 and 1365 ppm) for 2 d. During gas exchange measurements, slightly lower C_i levels prevailed (136, 202, 304, 516 and 1282 ppm). Symbols: A_m , measured CO₂ assimilation; C_a , atmospheric CO₂ concentration; C_i , intercellular CO₂ concentration; $R_{a,p}$, respiration by and flux through the plastidial anaplerotic pathway; R_d , total day respiration; R_x , day respiration by processes other than the plastidial anaplerotic pathway; V_c , rubisco carboxylation; V_o , rubisco oxygenation. All panels show discrete data. Dashed lines were added to guide the eye.

mol ATP requires 14 mol H⁺ as derived from ATPase subunit composition (Seelert *et al.*, 2000), linear electron transport including Q cycling results in an ATP deficit at $C_a \approx 450$ ppm. In both cases, ATP deficits increase significantly both above and

below $C_a \approx 450$ ppm. This suggests that increasing flux through the plastidial anaplerotic pathway increases the requirement for ATP synthesis via cyclic electron transport around photosystem I. Assuming an H⁺-ATP synthesis ratio of 12 : 3, cyclic electron transport including Q cycling is not required when the plastidial anaplerotic pathway is inactive, but it may account for up to 17% of the rate of whole electron transport when this pathway is active. Assuming an H⁺-ATP synthesis ratio of 14 : 3, cyclic electron transport including Q cycling accounts for *c.* 20% of the rate of whole electron transport when the plastidial anaplerotic pathway is inactive and may increase to above 30% when this pathway is active. Thus, flux through the plastidial anaplerotic pathway may affect the light reactions of photosynthesis.

Discussion

Here, we expanded FvCB models by terms accounting for respiration and energy recycling by the plastidial anaplerotic pathway (Eqns 5 and 12). We fitted the model of RuBP-regeneration-limited assimilation to gas exchange data of sunflower leaves by adjusting day respiration. This approach and previous reports (Wieloch, 2022; Wieloch *et al.*, 2022a) challenge a longstanding FvCB modelling assumption, namely the treatment of day respiration as independent, constant term. If this assumption is false, then several FvCB-model-based methods require revision, including methods for estimating day respiration (e.g. Laisk, 1977) and mesophyll conductance (see below). Moreover, initial linear increases in A/C_i curves are commonly interpreted in terms of rubisco-limited assimilation (Farquhar *et al.*, 1980). Here, we propose RuBP-regeneration-limited assimilation and varying rates of respiration from the plastidial anaplerotic pathway as alternative explanation. Our modelling results suggest that the plastidial anaplerotic pathway can be an important player in plant carbon and energy metabolism affecting properties such as the rate of day respiration, net CO₂ assimilation, net carboxylation, net oxygenation (photorespiration), RuBP regeneration, NADPH availability, the ATP : NADPH demand ratio of plastidial carbon metabolism, and probably the contribution of the cyclic electron pathway to supplying ATP (Figs 5–7; Tables 2–4).

Consistent evidence in support of flux through the plastidial anaplerotic pathway

According to our gas exchange analysis, flux through the plastidial anaplerotic pathway proceeds at 0, 2.44 and 2.75 $\mu\text{mol m}^{-2} \text{s}^{-1}$ at $C_a \approx 450$, 280 and 180 ppm, respectively (Table 2, Fig. 5a). That is, flux increases with decreasing C_a from *c.* 0% over *c.* 29% to *c.* 54% relative to the rate of net CO₂ assimilation (Fig. 6a). This is consistent with regulatory properties of the pathway and previously reported flux estimates as discussed next.

Flux through the plastidial anaplerotic pathway is controlled at its first enzyme, glucose-6-phosphate dehydrogenase (G6PD, Fig. 1). Under illumination, G6PD is downregulated by a thioredoxin-dependent mechanism (Née *et al.*, 2009). However, downregulation can be reversed allosterically by G6P (Cossar *et al.*, 1984; Preiser *et al.*, 2019). Under medium-to-high C_a , the

Table 3 Energy recovery by the plastidial anaplerotic pathway and associated CO₂ assimilation in sunflower leaves.

C _a (ppm)	Φ	R _{a,p} ^a (μmol m ⁻² s ⁻¹)	abs. NADPH input ^b (μmol m ⁻² s ⁻¹)	abs. NADPH output ^c (μmol m ⁻² s ⁻¹)	rel. NADPH recovery ^d	abs. CO ₂ recovery (A _{a,p}) ^e (μmol m ⁻² s ⁻¹)	rel. CO ₂ recovery ^f	ΔA _j (μmol m ⁻² s ⁻¹)	ΔA _j /R _{a,p}
c. 180	0.72	2.75	9.46	5.51	0.58	1.03	0.37	1.73	0.63
c. 280	0.49	2.44	7.27	4.89	0.67	1.24	0.51	1.20	0.49
c. 450	0.32	0	0	0	–	0	–	0.00	–
c. 700	0.18	0.30	0.70	0.60	0.84	0.23	0.77	0.07	0.23
c. 1500	0.07	0.87	1.86	1.73	0.93	0.78	0.90	0.09	0.10

Plants were grown in a glasshouse at an atmospheric CO₂ concentration (C_a) of c. 450 ppm and then moved to growth chambers. After a day in darkness to drain the starch reserves, the plants were grown at different levels of C_a (180, 280, 450, 700 and 1500 ppm) corresponding to different levels of intercellular CO₂ concentration (C_i = 140, 206, 328, 531 and 1365 ppm) for 2 d. During gas exchange measurements, slightly lower C_i levels prevailed (136, 202, 304, 516 and 1282 ppm). Symbols: A_{a,p}, CO₂ assimilation with electrons recovered by the plastidial anaplerotic pathway in the form of nicotinamide adenine dinucleotide phosphate (NADPH); R_{a,p}, respiration by the plastidial anaplerotic pathway; ΔA_j, absolute effect of flux through the plastidial anaplerotic pathway on the A/C_i curve (ribulose 1,5-bisphosphate (RuBP)-regeneration-limited case); Φ, oxygenation-to-carboxylation ratio of rubisco.

^aEstimates based on Eqn 13 with R_x values from Table 2.

^b(2 + 2Φ)R_{a,p} (derivation of Eqn 7, 2 electrons per NADPH).

^c2R_{a,p} (see Fig. 1).

^dNADPH output/NADPH input.

^eEstimates based on Eqn 11.

^fA_{a,p}/R_{a,p}.

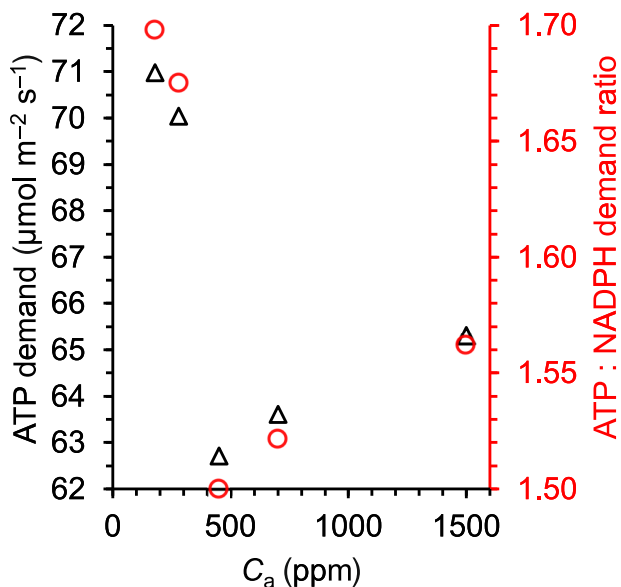


Fig. 7 Energy demand from the light reactions of photosynthesis at varying atmospheric CO₂ concentration (C_a) in sunflower leaves. Black triangles: adenosine triphosphate (ATP) demand. Red circles: ATP : NADPH demand ratio. Energy fluxes were estimated based on carbon flux estimates from modelling ribulose 1,5-bisphosphate (RuBP)-regeneration-limited CO₂ assimilation. The model considers the Calvin–Benson cycle, the photorespiration cycle, the plastidial anaplerotic pathway and respiration by processes other than the plastidial anaplerotic pathway. Plants were grown in a glasshouse at C_a ≈ 450 ppm and then moved to growth chambers. After a day in darkness to drain the starch reserves, plants were grown at different levels of C_a (180, 280, 450, 700 and 1500 ppm) corresponding to different levels of C_i (140, 206, 328, 531 and 1365 ppm) for 2 d. During gas exchange measurements, slightly lower C_i levels prevailed (136, 202, 304, 516 and 1282 ppm).

reaction catalysed by plastidial phosphoglucose isomerase (PGI) was found to be removed from equilibrium on the side of F6P (Schleucher *et al.*, 1999; Wieloch, 2022; Wieloch *et al.*, 2022a)

resulting in low G6P concentration (Dietz, 1985; Gerhardt *et al.*, 1987; Kruckeberg *et al.*, 1989). With shifts to low C_a, the PGI reaction moves towards equilibrium (Wieloch, 2022; Wieloch *et al.*, 2022a) and plastidial G6P concentrations increase (Dietz, 1985). Furthermore, phosphorolytic starch breakdown increases with photorespiration providing additional G6P (dotted arrow in Fig. 1; Weise *et al.*, 2006). These mechanisms are consistent with reports of negligible flux through the anaplerotic pathway at medium C_a (low G6P concentration) and flux increases with decreasing C_a, increasing photorespiration and increasing drought (high G6P concentration; Wieloch *et al.*, 2018, 2022a,b; Wieloch, 2022).

Previously, we estimated flux through the plastidial anaplerotic pathway in the leaves studied here proceeds at 0%, > 5% and > 7% relative to the rate of net CO₂ assimilation at C_a ≈ 450, 280 and 180 ppm, respectively (Wieloch, 2022; Wieloch *et al.*, 2022a). These estimates are based on a hydrogen isotope signal in starch introduced in the starch biosynthesis pathway at the level of G6P H¹. G6P may be converted back to fructose 6-phosphate (F6P) by PGI, and F6P may leave the starch biosynthesis pathway via transketolase. Combinedly, G6P to F6P conversion and F6P use by transketolase can be expected to cause washout of the isotope signal from the starch biosynthesis pathway. As evident from an isotope signal at starch glucose H², the plastidial PGI reaction is strongly removed from equilibrium on the side of F6P at C_a ≥ 450 ppm (Wieloch, 2022; Wieloch *et al.*, 2022a). This is thought to impede back conversion of G6P to F6P and concomitant signal washout. However, the PGI reaction moves progressively towards equilibrium as C_a decreases below c. 450 ppm (Wieloch, 2022; Wieloch *et al.*, 2022a). This is thought to result in increasing back conversion of G6P to F6P and signal washout. Thus, increasing offsets between R_{a,p} estimates from isotope

Table 4 Effects of the plastidial anaplerotic pathway on electron transport in sunflower leaves.

H ⁺ -ATP ratio of ATPase	12/3					14/3				
C _a (ppm)	180	280	450	700	1500	180	280	450	700	1500
LET (μmol m ⁻² s ⁻¹)	83.6	83.6	83.6	83.6	83.6	83.6	83.6	83.6	83.6	83.6
ATP demand (μmol m ⁻² s ⁻¹)	71.0	70.0	62.7	63.6	65.3	71.0	70.0	62.7	63.6	65.3
ATP from LET (μmol m ⁻² s ⁻¹)	62.7	62.7	62.7	62.7	62.7	53.8	53.8	53.8	53.8	53.8
ATP deficit (μmol m ⁻² s ⁻¹)	8.3	7.3	0.0	0.9	2.6	17.2	16.3	9.0	9.9	11.6
CET (μmol m ⁻² s ⁻¹)	16.5	14.7	0.0	1.8	5.2	40.2	38.0	20.9	23.0	27.0
CET/(CET + LET)	0.17	0.15	0.0	0.02	0.06	0.32	0.31	0.20	0.22	0.24

Plants were grown in a glasshouse at an atmospheric CO₂ concentration (C_a) of c. 450 ppm and then moved to growth chambers. After a day in darkness to drain the starch reserves, the plants were grown at different levels of C_a (180, 280, 450, 700 and 1500 ppm) for 2 d. Gas exchange measurements were performed at a light intensity of 300 μmol photons m⁻² s⁻¹. Estimations pertaining to linear and cyclic electron transport (LET and CET, both including Q cycling) assumed transmembrane transport of 3 and 2 H⁺ per electron, respectively. Synthesis of 3 mol adenosine triphosphate (ATP) by ATPase was assumed to require either 14 or 12 mol H⁺ (according to Seelert *et al.*, 2000 and Steigmiller *et al.*, 2008, respectively). Processes not considered include the water–water cycle (affects the ATP : NADPH supply ratio of electron transport), GAP/3PGA cycles and the chloroplast malate valve (affect ATP : NADPH demand ratios of carbon metabolism). NADPH, nicotinamide adenine dinucleotide phosphate.

and gas exchange analysis with decreasing C_a probably derive from increasing washout of the isotope signal.

Physiological function of flux through the plastidial anaplerotic pathway

Flux through the anaplerotic pathway lowers net CO₂ assimilation below theoretically possible values (Fig. 4b, black dots vs red line). As a result of this flux, sunflower leaves merely achieve c. 88% and c. 75% of their theoretical assimilatory potential at C_a ≈ 280 ppm and c. 180 ppm, respectively. Similarly, the anaplerotic pathway recovers only part of the energy it consumes (Fig. 5b; Table 3), and energy dissipation is surely not physiologically beneficial under RuBP-regeneration-limited conditions. Thus, for the conditions and period studied here, the anaplerotic pathway appears to be detrimental for both leaf carbon and energy balances.

However, the sunflowers studied here were raised at C_a ≈ 450 ppm. Hence, heterotrophic carbon demands were probably adapted to carbon inputs at C_a ≈ 450 ppm. Moving the plants into low-C_a environments may have caused divergences from the previously established whole-plant steady state with leaf carbon exports exceeding net CO₂ assimilation (Fig. 1). This source limitation may have resulted in excess export of triose phosphates from chloroplasts. Plastidial triose phosphate shortage would impede RuBP regeneration. To maintain the supply of RuBP, plants may inject G6P from phosphorolytic starch breakdown into the CBC (Weise *et al.*, 2006). G6P-derived carbon can enter the CBC via transketolase without respiratory carbon loss and via the anaplerotic pathway with respiratory carbon loss. However, transketolase and other enzymes in the regeneration part of the CBC require triose phosphate. When RuBP regeneration is impeded by triose phosphate shortage, the anaplerotic pathway may help to ensure RuBP supply.

RuBP may undergo either oxygenation or carboxylation at rubisco. With decreasing C_a, oxygenation becomes substantial (Table 3, c. 1 and c. 1.5 mol RuBP oxygenation per 2 mol RuBP carboxylation at C_a ≈ 280 ppm and c. 180 ppm, respectively). Thus, much of the anaplerotically supplied RuBP feeds into photorespiration. As proposed previously, maintaining photorespiration through inputs of RuBP might make sense

physiologically in the context of the concept of photorespiration-linked *de novo* nitrogen assimilation (Wieloch *et al.*, 2022a). Reportedly, photorespiration rate correlates positively with the rate of *de novo* nitrate assimilation (Bloom, 2015), and it seems plausible that plants would shift metabolism towards nitrogen assimilation when carbon assimilation is impeded (at low C_a). Assimilated nitrogen may support *de novo* protein synthesis, which may result in increased photosynthetic capacity at the enzyme level and help to overcome source limitations.

In this context, it is interesting to note that mutants incapable of phosphorolytic starch breakdown show severe phenotypes, especially under drought (dotted arrow in Fig. 1; Zeeman *et al.*, 2004). This was explained by the loss of G6P injection from starch into the CBC at night (Zeeman *et al.*, 2004). Based on findings presented here and previously, impaired G6P injection during the day may contribute to this phenotype (Wieloch *et al.*, 2018, 2022a, 2022b). Lastly, G6P injection from starch into the CBC by the anaplerotic pathway may support photosynthetic induction (see below).

Metabolic origin of day respiration at high C_a

In our gas exchange analysis, respiration by the plastidial anaplerotic pathway was fixed at 0%, 2% and 5% relative to the rate of net CO₂ assimilation at C_a ≈ 450, 700 and 1500 ppm, respectively (Fig. 5a; Table 2). These R_{a,p} estimates come from a previously published isotope analysis of the samples studied here (Wieloch, 2022). Increases in R_{a,p} above C_a ≈ 450 ppm are consistent with regulatory properties of the plastidial anaplerotic pathway (Wieloch, 2022). Towards high C_a, plastidial G6P concentrations increase with net CO₂ assimilation (Dietz, 1985). This can be expected to cause increased G6PD activity and flux through the plastidial anaplerotic pathway (see above). Note, in contrast to the low-C_a case (see above), R_{a,p} increases at high C_a are not caused by PGI regulation (Wieloch, 2022).

Here, we estimated that respiration by processes other than the plastidial anaplerotic pathway proceeds at 0.96, 1.08 and 1.38 μmol m⁻² s⁻¹ at C_a ≈ 450, 700 and 1500 ppm, respectively (Fig. 5a; Table 2). These increases are consistent with regulatory

properties of the cytosolic OPPP (Wieloch, 2022), which has recently been identified as a major source of day respiration (Xu *et al.*, 2022). Flux through the cytosolic OPPP and associated respiration is controlled at the level of the first OPPP enzyme, G6PD (Fig. 1). Under illumination, cytosolic G6PD activity increases with glucose concentration through *de novo* enzyme synthesis (Hauschild & von Schaewen, 2003). In line with this, respiration at 5°C was shown to increase with glucose concentration and overall leaf soluble sugar concentration (Tjoelker *et al.*, 2009; Wieloch, 2022). Generally, increasing C_a results in increasing leaf soluble sugar concentration (Ainsworth & Long, 2005) and may thus cause increasing respiration by the cytosolic OPPP.

Does g_m vary with C_a ?

Using the online carbon isotope discrimination method and/or the variable J method (Evans *et al.*, 1986; Harley *et al.*, 1992), several authors reported nonlinear relationships between g_m and C_a with similar patterns across different species including sunflower (Flexas *et al.*, 2007; Hassiotou *et al.*, 2009; Vrábl *et al.*, 2009; Xiong *et al.*, 2015). As C_a increases, g_m initially increases up to a change point beyond which it decreases again. This response is strikingly similar to the C_a -response of day respiration reported here. As C_a increases, $R_{a,p}$ initially decreases up to a change point beyond which it increases again along with R_x (Fig. 5a; Table 2). Day respiration and g_m have opposite effects on net CO₂ assimilation. That is, both processes could explain offsets between measured and theoretically possible values of net CO₂ assimilation (Fig. 4b, black dots vs red line). However, changes in day respiration estimated here based on gas exchange analysis are corroborated by results from an independent isotope analysis (Wieloch, 2022; Wieloch *et al.*, 2022a). Furthermore, underlying metabolic mechanisms seem straight forward (see above). By contrast, mechanisms underlying the C_a -response of g_m have remained unclear despite considerable research interest over the past three decades (Nadal *et al.*, 2021). Several authors suggested that much of the observed variability of g_m may be due to methodological shortcomings (Tholen *et al.*, 2012; Gu & Sun, 2014; Yin *et al.*, 2020; Nadal *et al.*, 2021). Our results corroborate this viewpoint. Therefore, we recommend modifying the variable J method to allow for variability in day respiration. Furthermore, we recommend modifying the online carbon isotope discrimination method to allow for variability in isotope fractionation of photorespiration and day respiration. Adequate (yet probably challenging) parameterisation of these models may show whether g_m varies with C_a . Similarly, considering day respiratory variability may advance the discussion about relationships between g_m and other environmental variables (drought, irradiance, ozone and temperature; see Nadal *et al.*, 2021).

Respiration by the plastidial anaplerotic pathway during photosynthetic induction

Flux through the plastidial anaplerotic pathway and associated respiration depends on G6PD activity. Plastidial G6PD is inhibited by reduced thioredoxin (Née *et al.*, 2009). However,

reduction of the plastidial thioredoxin pool after illumination is not instantaneous but builds up over the course of several minutes (Scheibe, 1981). This was shown to result in a gradual activation of plastidial malate dehydrogenase (Scheibe, 1981). Similarly, gradual inhibition of plastidial G6PD can be expected. Thus, flux through the plastidial anaplerotic pathway may persist over the course of several minutes after illumination decreasing from initially higher to lower levels. This would affect day respiration, net CO₂ assimilation, NADPH supply, the isotopic composition of respired CO₂, etc. Future studies on the variability of photosynthetic parameters such as g_m during photosynthetic induction (cf. Kaiser *et al.*, 2017; Sakoda *et al.*, 2021; Liu *et al.*, 2022) are encouraged to consider this as a possibility.

Does day respiration explain part of the A/C_i curve drop at high C_a ?

If R_d is held constant, rubisco-limited and RuBP-regeneration-limited net CO₂ assimilation modelled by the canonical FvCB equations increase continuously with increasing C_a (Farquhar *et al.*, 1980). However, especially under high light, measured A/C_i curves are frequently seen to level out or even decline at high C_a (e.g. Sharkey, 1985; Harley & Sharkey, 1991). According to our analysis, day respiration increases from *c.* 8% relative to the rate of net CO₂ assimilation at $C_a \approx 450$ ppm to *c.* 13% at $C_a \approx 1500$ ppm (Fig. 5a; Table 2). This is consistent with positive responses of R_d to C_a reported by some authors (e.g. Wang *et al.*, 2001). By contrast, other authors reported R_d is independent of C_a (e.g. Ayub *et al.*, 2011).

Increases in R_d are consistent with regulatory properties of both the plastidial and cytosolic OPPP (see above). As C_a increases from medium to high values, plastidial G6P concentrations and leaf soluble sugar concentrations increase (Dietz, 1985; Ainsworth & Long, 2005). This can be expected to activate both plastidial and cytosolic G6PD (Cossar *et al.*, 1984; Hauschild & von Schaewen, 2003; Preiser *et al.*, 2019), increase respiration by the plastidial and cytosolic OPPP and explain part of the A/C_i curve drop at high C_a . Furthermore, it may explain part of the lower-than-expected stimulation of net CO₂ assimilation by increasing C_a (Wieloch, 2022). However, high sink strengths (e.g. in vigorously growing plants) may counteract the build-up of leaf soluble sugar concentrations and respiration by the plastidial and cytosolic OPPP. This may explain why some studies found R_d increases at high C_a whereas others did not.

Model criticism and future research directions

Generally, modelling net CO₂ assimilation by FvCB-type models relies on numerous assumptions (Tcherkez & Limami, 2019), and the present study is no exception. For instance, our models assume that photorespiration is a closed cycle. However, some of the carbon entering photorespiration may actually be diverted into other pathways such as *de novo* nitrogen assimilation (Busch *et al.*, 2018). Similarly, in our A_j model (Eqn 12), the CBC and photorespiration are assumed to consume all energy. However, part of the available energy can be expected to be utilised by other

plastidial processes such as the reduction of nitrite to ammonia (Buchanan *et al.*, 2015) or NAD(P)H shuttling to other cell compartments (Scheibe, 2004). Furthermore, our modelling assumes constant absolute R_x at $C_a \leq 450$ ppm (Table 2). However, leaf soluble sugar concentration may decrease with decreasing C_a (Ainsworth & Long, 2005). This may cause a reduction in G6PD activity and respiration by the cytosolic OPPP (Hauschild & von Schaewen, 2003). Lastly, our modelling relies on sunflower parameter estimates from the literature. Such estimates can vary strongly among species (Orr *et al.*, 2016), and there is a lack of data on parameter variability in sunflower. Considering these uncertainties, results reported here require validation (Supporting Information Notes S1 including Fig. S1; Table S1). Hence, we recommend follow-up studies that combine gas exchange measurements, isotope measurements and model parameter measurements from the same plants.

That said, our estimate of R_x at $C_a \approx 450$ ppm is consistent with previously reported estimates (Tcherkez *et al.*, 2017). Furthermore, estimates of flux through the plastidial anaplerotic pathway from gas exchange analyses presented here are qualitatively consistent with previously reported isotope-derived estimates (Wieloch, 2022; Wieloch *et al.*, 2022a). Lastly, all estimates of day respiration are consistent with regulatory properties of the plastidial and cytosolic anaplerotic pathway. Hence, we hope that the model extensions and ideas presented here will help to advance photosynthesis modelling. Future research directions of interest include the study of $R_{a,p}$ at and below the CO_2 compensation point, and attempts to model $R_{a,p}$ as function of underlying biochemical mechanisms.

Acknowledgements

We thank Prof. Jun Yu (Umeå University) for helpful discussions and bioRxiv (Cold Spring Harbor Laboratory, NY, USA) for publishing preprints of the present paper (doi: 10.1101/2021.07.30.454461).

Competing interests

None declared.

Author contributions

TW conceived the study, led the research, expanded FvCB models and analysed the data. AA and JS prepared samples and acquired gas exchange data. TW wrote the paper with input from all authors. TW revised the paper.

ORCID

Angela Augusti  <https://orcid.org/0000-0002-9591-693X>
 Jürgen Schleucher  <https://orcid.org/0000-0002-4815-3466>
 Thomas Wieloch  <https://orcid.org/0000-0001-9162-2291>

Data availability

Data are available in the article.

References

- Ainsworth EA, Long SP. 2005. What have we learned from 15 years of free-air CO_2 enrichment (FACE)? A meta-analytic review of the responses of photosynthesis, canopy properties and plant production to rising CO_2 . *New Phytologist* 165: 351–372.
- Ayub G, Smith RA, Tissue DT, Atkin OK. 2011. Impacts of drought on leaf respiration in darkness and light in *Eucalyptus saligna* exposed to industrial-age atmospheric CO_2 and growth temperature. *New Phytologist* 190: 1003–1018.
- Bloom AJ. 2015. Photorespiration and nitrate assimilation: a major intersection between plant carbon and nitrogen. *Photosynthesis Research* 123: 117–128.
- Buchanan BB, Gruissem W, Jones RL, eds. 2015. *Biochemistry and molecular biology of plants*. Chichester, UK: John Wiley & Sons.
- Busch FA, Sage RF, Farquhar GD. 2018. Plants increase CO_2 uptake by assimilating nitrogen via the photorespiratory pathway. *Nature Plants* 4: 46–54.
- von Caemmerer S. 2000. *Biochemical models of leaf photosynthesis*. Collingwood: CSIRO, Vic., Australia.
- Cossar JD, Rowell P, Stewart WDP. 1984. Thioredoxin as a modulator of glucose-6-phosphate dehydrogenase in a N_2 -fixing cyanobacterium. *Microbiology* 130: 991–998.
- Dietz K-J. 1985. A possible rate-limiting function of chloroplast hexosemonophosphate isomerase in starch synthesis of leaves. *Biochimica et Biophysica Acta* 839: 240–248.
- Ehlers I, Augusti A, Betson TR, Nilsson MB, Marshall JD, Schleucher J. 2015. Detecting long-term metabolic shifts using isotopomers: CO_2 -driven suppression of photorespiration in C_3 plants over the 20th century. *Proceedings of the National Academy of Sciences, USA* 112: 15585–15590.
- Eicks M, Maurino V, Knappe S, Flügge U-I, Fischer K. 2002. The plastidic pentose phosphate translocator represents a link between the cytosolic and the plastidic pentose phosphate pathways in plants. *Plant Physiology* 128: 512–522.
- Evans J. 1987. The dependence of quantum yield on wavelength and growth irradiance. *Functional Plant Biology* 14: 69–79.
- Evans JR. 1989. Photosynthesis and nitrogen relationships in leaves of C_3 plants. *Oecologia* 78: 9–19.
- Evans JR, Farquhar GD, Sharkey TD, Berry JA. 1986. Carbon isotope discrimination measured concurrently with gas exchange to investigate CO_2 diffusion in leaves of higher plants. *Australian Journal of Plant Physiology* 13: 281–292.
- Farquhar G, Wong S. 1984. An empirical model of stomatal conductance. *Functional Plant Biology* 11: 191–210.
- Farquhar GD, Caemmerer S, Berry JA. 1980. A biochemical model of photosynthetic CO_2 assimilation in leaves of C_3 species. *Planta* 149: 78–90.
- Farquhar GD, von Caemmerer S. 1982. Modelling of photosynthetic response to environmental conditions. In: Lange OL, Nobel PS, Osmond CB, Ziegler H, eds. *Physiological plant ecology II: water relations and carbon assimilation*. Berlin & Heidelberg, Germany: Springer, 549–587.
- Flexas J, Diaz-Espejo A, Galmé SJ, Kaldenhoff R, Medrano H, Ribas-Carbo M. 2007. Rapid variations of mesophyll conductance in response to changes in CO_2 concentration around leaves. *Plant, Cell & Environment* 30: 1284–1298.
- Genkov T, Meyer M, Griffiths H, Spreitzer RJ. 2010. Functional hybrid Rubisco enzymes with plant small subunits and algal large subunits. *Journal of Biological Chemistry* 285: 19833–19841.
- Gerhardt R, Stitt M, Heldt HW. 1987. Subcellular metabolite levels in spinach leaves: regulation of sucrose synthesis during diurnal alterations in photosynthetic partitioning. *Plant Physiology* 83: 399–407.
- Gu L, Sun Y. 2014. Artefactual responses of mesophyll conductance to CO_2 and irradiance estimated with the variable J and online isotope discrimination methods. *Plant, Cell & Environment* 37: 1231–1249.
- Harley PC, Loreto F, Di Marco G, Sharkey TD. 1992. Theoretical considerations when estimating the mesophyll conductance to CO_2 flux by analysis of the response of photosynthesis to CO_2 . *Plant Physiology* 98: 1429–1436.
- Harley PC, Sharkey TD. 1991. An improved model of C_3 photosynthesis at high CO_2 : reversed O_2 sensitivity explained by lack of glycerate reentry into the chloroplast. *Photosynthesis Research* 27: 169–178.

- Hassiotou F, Ludwig M, Renton M, Veneklaas EJ, Evans JR. 2009. Influence of leaf dry mass per area, CO₂, and irradiance on mesophyll conductance in sclerophylls. *Journal of Experimental Botany* 60: 2303–2314.
- Hauschild R, von Schaewen A. 2003. Differential regulation of glucose-6-phosphate dehydrogenase isoenzyme activities in potato. *Plant Physiology* 133: 47–62.
- Jacob J, Lawlor DW. 1991. Stomatal and mesophyll limitations of photosynthesis in phosphate deficient sunflower, maize and wheat plants. *Journal of Experimental Botany* 42: 1003–1011.
- Kaiser E, Kromdijk J, Harbinson J, Heuvelink E, Marcelis LFM. 2017. Photosynthetic induction and its diffusional, carboxylation and electron transport processes as affected by CO₂ partial pressure, temperature, air humidity and blue irradiance. *Annals of Botany* 119: 191–205.
- Kruckeberg AL, Neuhaus HE, Feil R, Gottlieb LD, Stitt M. 1989. Decreased-activity mutants of phosphoglucose isomerase in the cytosol and chloroplast of *Clarkia xantiana*. *The Biochemical Journal* 261: 457–467.
- Laisk A. 1977. *Kinetics of photosynthesis and photorespiration in C₃ plants*. Moscow, Russia: Nauka.
- Laisk A, Edwards GE. 1997. CO₂ and temperature-dependent induction in C₄ photosynthesis: an approach to the hierarchy of rate-limiting processes. *Functional Plant Biology* 24: 505–516.
- Liu T, Barbour MM, Yu D, Rao S, Song X. 2022. Mesophyll conductance exerts a significant limitation on photosynthesis during light induction. *New Phytologist* 233: 360–372.
- Nadal M, Carriqui M, Flexas J. 2021. Chapter 3 Mesophyll conductance to CO₂ diffusion in a climate change scenario: effects of elevated CO₂, temperature and water stress. In: Becklin KM, Ward JK, Way DA, eds. *Photosynthesis, respiration, and climate change*. Cham, Switzerland: Springer International, 49–78.
- Née G, Zaffagnini M, Trost P, Issakidis-Bourguet E. 2009. Redox regulation of chloroplastic glucose-6-phosphate dehydrogenase: a new role for f-type thioredoxin. *FEBS Letters* 583: 2827–2832.
- Orr DJ, Alcântara A, Kapralov MV, Andralojc PJ, Carmo-Silva E, Parry MAJ. 2016. Surveying Rubisco diversity and temperature response to improve crop photosynthetic efficiency. *Plant Physiology* 172: 707–717.
- Preiser AL, Fisher N, Banerjee A, Sharkey TD. 2019. Plastidic glucose-6-phosphate dehydrogenases are regulated to maintain activity in the light. *Biochemical Journal* 476: 1539–1551.
- Sakoda K, Yamori W, Groszmann M, Evans JR. 2021. Stomatal, mesophyll conductance, and biochemical limitations to photosynthesis during induction. *Plant Physiology* 185: 146–160.
- Schäufele R, Santrucek J, Schnyder H. 2011. Dynamic changes of canopy-scale mesophyll conductance to CO₂ diffusion of sunflower as affected by CO₂ concentration and abscisic acid. *Plant, Cell & Environment* 34: 127–136.
- Scheibe R. 1981. Thioredoxin_m in pea chloroplasts: concentration and redox state under light and dark conditions. *FEBS Letters* 133: 301–304.
- Scheibe R. 2004. Malate valves to balance cellular energy supply. *Physiologia Plantarum* 120: 21–26.
- Schleucher J, Vanderveer P, Markley JL, Sharkey TD. 1999. Intramolecular deuterium distributions reveal disequilibrium of chloroplast phosphoglucose isomerase. *Plant, Cell & Environment* 22: 525–533.
- Seelert H, Poetsch A, Dencher NA, Engel A, Stahlberg H, Müller DJ. 2000. Proton-powered turbine of a plant motor. *Nature* 405: 418–419.
- Sharkey TD. 1985. O₂-insensitive photosynthesis in C₃ plants: its occurrence and a possible explanation. *Plant Physiology* 78: 71–75.
- Sharkey TD, Berry JA, Raschke K. 1985. Starch and sucrose synthesis in *Phaseolus vulgaris* as affected by light, CO₂, and abscisic acid. *Plant Physiology* 77: 617–620.
- Sharkey TD, Weise SE. 2016. The glucose 6-phosphate shunt around the Calvin–Benson cycle. *Journal of Experimental Botany* 67: 4067–4077.
- Steigmiller S, Turina P, Gräber P. 2008. The thermodynamic H⁺/ATP ratios of the H⁺-ATPsynthases from chloroplasts and *Escherichia coli*. *Proceedings of the National Academy of Sciences, USA* 105: 3745–3750.
- Taira M, Valtersson U, Burkhardt B, Ludwig RA. 2004. *Arabidopsis thaliana* GLN2-encoded glutamine synthetase is dual targeted to leaf mitochondria and chloroplasts. *Plant Cell* 16: 2048–2058.
- Tcherkez G, Gauthier P, Buckley TN, Busch FA, Barbour MM, Bruhn D, Heskell MA, Gong XY, Crous KY, Griffin K *et al.* 2017. Leaf day respiration: low CO₂ flux but high significance for metabolism and carbon balance. *New Phytologist* 216: 986–1001.
- Tcherkez G, Limami AM. 2019. Net photosynthetic CO₂ assimilation: more than just CO₂ and O₂ reduction cycles. *New Phytologist* 223: 520–529.
- Tholen D, Ethier G, Genty B, Pepin S, Zhu X-G. 2012. Variable mesophyll conductance revisited: theoretical background and experimental implications. *Plant, Cell & Environment* 35: 2087–2103.
- Tjoelker MG, Oleksyn J, Lorenc-Plucinska G, Reich PB. 2009. Acclimation of respiratory temperature responses in northern and southern populations of *Pinus banksiana*. *New Phytologist* 181: 218–229.
- Vrábl D, Vašková M, Hronková M, Flexas J, Šantrůček J. 2009. Mesophyll conductance to CO₂ transport estimated by two independent methods: effect of variable CO₂ concentration and abscisic acid. *Journal of Experimental Botany* 60: 2315–2323.
- Walker AP, Beckerman AP, Gu L, Kattge J, Cernusak LA, Domingues TF, Scales JC, Wohlfahrt G, Wullschlegel SD, Woodward FI. 2014. The relationship of leaf photosynthetic traits – V_{cmax} and J_{max} – to leaf nitrogen, leaf phosphorus, and specific leaf area: a meta-analysis and modeling study. *Ecology and Evolution* 4: 3218–3235.
- Wang X, Lewis JD, Tissue DT, Seemann JR, Griffin KL. 2001. Effects of elevated atmospheric CO₂ concentration on leaf dark respiration of *Xanthium strumarium* in light and in darkness. *Proceedings of the National Academy of Sciences, USA* 98: 2479–2484.
- Weise SE, Schrader SM, Kleinbeck KR, Sharkey TD. 2006. Carbon balance and circadian regulation of hydrolytic and phosphorylytic breakdown of transitory starch. *Plant Physiology* 141: 879–886.
- Wieloch T. 2021. The next phase in the development of ¹³C isotopically nonstationary metabolic flux analysis. *Journal of Experimental Botany* 72: 6087–6090.
- Wieloch T. 2022. High atmospheric CO₂ concentration causes increased respiration by the oxidative pentose phosphate pathway in chloroplasts. *New Phytologist* 235: 1310–1314.
- Wieloch T, Augusti A, Schleucher J. 2022a. Anaplerotic flux into the Calvin–Benson cycle. Hydrogen isotope evidence for *in vivo* occurrence in C₃ metabolism. *New Phytologist* 234: 405–411.
- Wieloch T, Ehlers I, Yu J, Frank D, Grabner M, Gessler A, Schleucher J. 2018. Intramolecular ¹³C analysis of tree rings provides multiple plant ecophysiology signals covering decades. *Scientific Reports* 8: 5048.
- Wieloch T, Grabner M, Augusti A, Serk H, Ehlers I, Yu J, Schleucher J. 2022b. Metabolism is a major driver of hydrogen isotope fractionation recorded in tree-ring glucose of *Pinus nigra*. *New Phytologist* 234: 449–461.
- Wieloch T, Sharkey TD. 2022. Compartment-specific energy requirements of photosynthetic carbon metabolism in *Camelina sativa* leaves. *Planta* 255: 103.
- Wullschlegel SD. 1993. Biochemical limitations to carbon assimilation in C₃ plants. A retrospective analysis of the A/C_i curves from 109 species. *Journal of Experimental Botany* 44: 907–920.
- Xiong D, Liu X, Liu L, Douthe C, Li Y, Peng S, Huang J. 2015. Rapid responses of mesophyll conductance to changes of CO₂ concentration, temperature and irradiance are affected by N supplements in rice. *Plant, Cell & Environment* 38: 2541–2550.
- Xu Y, Fu X, Sharkey TD, Shachar-Hill Y, Walker BJ. 2021. The metabolic origins of non-photorespiratory CO₂ release during photosynthesis: a metabolic flux analysis. *Plant Physiology* 186: 297–314.
- Xu Y, Wieloch T, Kaste JAM, Shachar-Hill Y, Sharkey TD. 2022. Reimport of carbon from cytosolic and vacuolar sugar pools into the Calvin–Benson cycle explains photosynthesis labeling anomalies. *Proceedings of the National Academy of Sciences, USA* 119: e2121531119.
- Yin X, van der Putten PEL, Belay D, Struik PC. 2020. Using photorespiratory oxygen response to analyse leaf mesophyll resistance. *Photosynthesis Research* 144: 85–99.
- Zeeman SC, Thorneycroft D, Schupp N, Chapple A, Weck M, Dunstan H, Haldimann P, Bechtold N, Smith AM, Smith SM. 2004. Plastidial α-glucan phosphorylase is not required for starch degradation in *Arabidopsis* leaves but has a role in the tolerance of abiotic stress. *Plant Physiology* 135: 849–858.

Supporting Information

Additional Supporting Information may be found online in the Supporting Information section at the end of the article.

Fig. S1 Net CO₂ assimilation (A) of sunflower leaves as function of intercellular CO₂ concentration (C_i).

Notes S1 Discussion of model parameter estimates including sensitivity analyses.

Table S1 Sensitivity of $R_{a,p}$ and R_x estimates to changes in J_{max} .

Please note: Wiley is not responsible for the content or functionality of any Supporting Information supplied by the authors. Any queries (other than missing material) should be directed to the *New Phytologist* Central Office.